PHYSICAL REVIEW B **88**, 064504 (2013)

Distinguishing $s^{\pm}$ and s^{++} electron pairing symmetries by neutron spin resonance in superconducting $NaFe_{0.935}Co_{0.045}As$

Chenglin Zhang,[1,2] H.-F. Li,[3,4] Yu Song,[1,2] Yixi Su,[5] Guotai Tan,[6,2] Tucker Netherton,[2] Caleb Redding,[2] Scott V. Carr,[1,2] Oleg Sobolev,[7] Astrid Schneidewind,[5,8] Enrico Faulhaber,[9,8] L. W. Harriger,[10] Shiliang Li,[11] Xingye Lu,[11] Dao-Xin Yao,[12] Tanmoy Das,[13] A. V. Balatsky,[13] Th. Brückel,[14] J. W. Lynn,[10] and Pengcheng Dai[1,2,11,*]

[1]*Department of Physics and Astronomy, Rice University, Houston, Texas 77005, USA*
[2]*Department of Physics and Astronomy, The University of Tennessee, Knoxville, Tennessee 37996-1200, USA*
[3]*Jülich Centre for Neutron Science JCNS, Forschungszentrum Jülich GmbH, Outstation at Institut Laue-Langevin, Boîte Postale 156, F-38042 Grenoble Cedex 9, France*
[4]*Institut für Kristallographie der RWTH Aachen, 52056 Aachen, Germany*
[5]*Jülich Centre for Neutron Science JCNS, Forschungszentrum Jülich GmbH, Outstation at MLZ, D-85747 Garching, Germany*
[6]*Department of Physics, Beijing Normal University, Beijing 100875, China*
[7]*Institut für Physikalische Chemie, Georg-August-Universität Göttingen, Tammannstrasse 6, 37077 Göttingen, Germany*
[8]*Forschungsneutronenquelle Heinz Maier-Leibnitz (FRM-II), TU München, D-85747 Garching, Germany*
[9]*Gemeinsame Forschergruppe HZB–TU Dresden, Helmholtz-Zentrum Berlin für Materialien und Energie, D-14109 Berlin, Germany*
[10]*NIST Center for Neutron Research, National Institute of Standards and Technology, Gaithersburg, Maryland 20899, USA*
[11]*Beijing National Laboratory for Condensed Matter Physics, Institute of Physics, Chinese Academy of Sciences, Beijing 100190, China*
[12]*State Key Laboratory of Optoelectronic Materials and Technology, Sun Yat-Sen University, Guangzhou 510275, China*
[13]*Theoretical Division, Los Alamos National Laboratory, Los Alamos, New Mexico, 87545, USA*
[14]*Jülich Centre for Neutron Science JCNS and Peter Grünberg Institut PGI, JARA-FIT, Forschungszentrum Jülich GmbH, 52425 Jülich, Germany*

(Received 17 May 2013; published 9 August 2013)

A determination of the superconducting (SC) electron pairing symmetry forms the basis for establishing a microscopic mechanism for superconductivity. For iron pnictide superconductors, the $s^{\pm}$-pairing symmetry theory predicts the presence of a sharp neutron spin resonance at an energy below the sum of hole and electron SC gap energies ($E \leqslant 2\Delta$) below T_c. On the other hand, the s^{++}-pairing symmetry expects a broad spin excitation enhancement at an energy above 2Δ below T_c. Although the resonance has been observed in iron pnictide superconductors at an energy below 2Δ consistent with the $s^{\pm}$-pairing symmetry, the mode has also been interpreted as arising from the s^{++}-pairing symmetry with $E \geqslant 2\Delta$ due to its broad energy width and the large uncertainty in determining the SC gaps. Here we use inelastic neutron scattering to reveal a sharp resonance at $E = 7$ meV in SC $NaFe_{0.935}Co_{0.045}As$ ($T_c = 18$ K). On warming towards T_c, the mode energy hardly softens while its energy width increases rapidly. By comparing with calculated spin-excitation spectra within the $s^{\pm}$ and s^{++}-pairing symmetries, we conclude that the ground-state resonance in $NaFe_{0.935}Co_{0.045}As$ is only consistent with the $s^{\pm}$ pairing, and is inconsistent with the s^{++}-pairing symmetry.

DOI: 10.1103/PhysRevB.88.064504 PACS number(s): 74.25.Ha, 74.70.−b, 78.70.Nx

I. INTRODUCTION

A determination of the superconducting (SC) electron pairing symmetry is an important step to establish a microscopic theory for high-transition temperature (high-T_c) superconductivity.[1] Since the discovery of iron pnictide superconductors,[2–4] a peculiar unconventional pairing state, where superconductivity arises from sign-reversed quasiparticle excitations between the isotropic hole and electron Fermi pockets near the Γ and M points, respectively, has been proposed.[5–7] A consequence of this so-called $s^{\pm}$-pairing state is that the sign-reversed quasiparticle excitations necessitate a sharp resonance in the spin excitations spectra (termed spin resonance) occurring below the sum of the hole and electron SC gap energies ($E \leqslant 2\Delta = \Delta_h + \Delta_e$) at the antiferromagnetic (AF) wave vector $\mathbf{Q}$ connecting the two Fermi surfaces [inset in Fig. 1(a)] below T_c.[8,9] The experimental discovery of the resonance by neutron scattering in hole and electron-doped $BaFe_2As_2$ iron pnictide superconductors[10–21] and iron chalcogenide Fe(Se,Te) family of materials[22–24] has provided strong evidence for the $s^{\pm}$-pairing symmetry. However, the neutron-scattering experiments on single crystals of $Ba_{0.67}K_{0.33}Fe_2As_2$,[11] $BaFe_{2-x}Co_xAs_2$,[13,15–17] and Fe(Se,Te) (Refs. 22–24) superconductors have also revealed that the resonance is rather broad in energy [Fig. 1(e)]. In addition, the SC gap energies 2Δ determined from the angle-resolved photoemission (ARPES) experiments for hole and electron-doped $BaFe_2As_2$ superconductors by different groups[25–28] can differ dramatically for even the same material, ranging from below to above the neutron spin-resonance energy [Fig. 1(e)], and these values can also be quite different from those estimated by specific-heat[29] and penetration depth measurements.[30] Because the superconducting gap values for the multiband iron pnictide superconductors are different for different bands,[25–28] the resonance energy is determined by the superconducting gaps in electron and hole bands contributing most to the quasiparticle nesting condition.[8,9] Therefore, the resonance in some materials may be broad in energy, and this has allowed some workers to argue that superconductivity

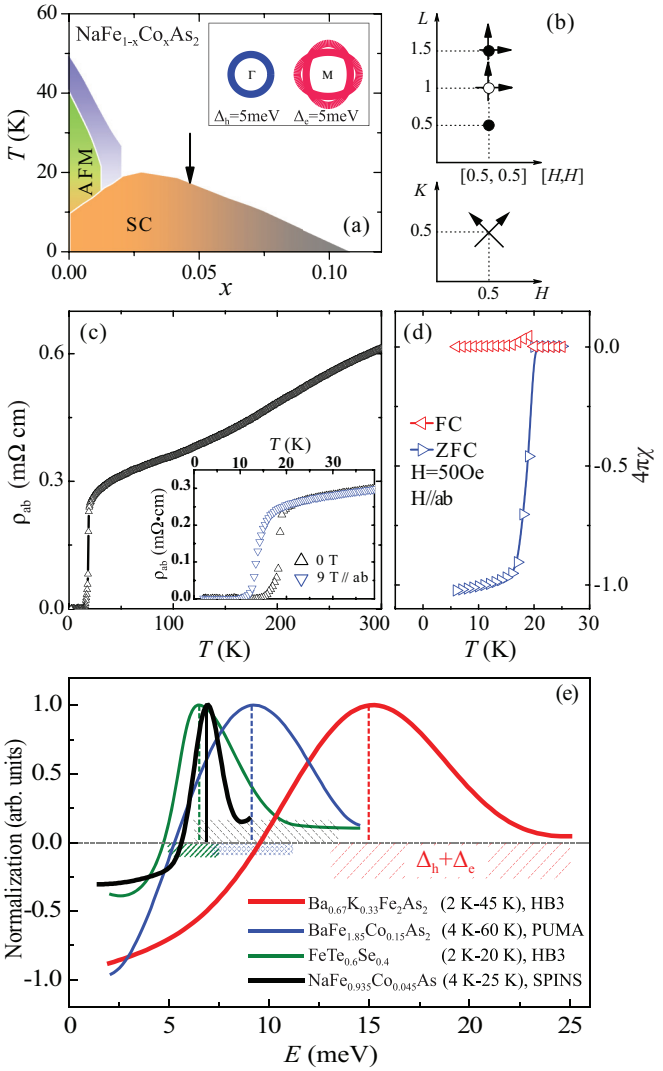

FIG. 1. (Color online) Phase diagram, Fermi surfaces, reciprocal space, transport, and susceptibility measurements. (a) The electronic phase diagram of $NaFe_{1-x}Co_xAs$, where the arrow indicates the Co-doping level of our samples. Inset shows the hole and electron Fermi pockets near Γ and M positions, respectively (Ref. 5). (b) Reciprocal space probed in the present experiment. The scan directions are shown as arrows. (c) Temperature dependence of the in-plane resistivity ρ_{ab} in $NaFe_{0.935}Co_{0.045}As$. The inset displays the low-T resistivity measured in zero field and 9 T. (d) The temperature dependence of the bulk susceptibility measured by dc magnetic susceptibility. (e) The schematics of neutron spin resonance for optimally hole (Ref. 11, red solid line) and electron (Ref. 15, blue solid line) iron pnictide superconductors. The green solid line shows results for $FeTe_{0.6}Se_{0.4}$ superconductor (Ref. 24) and black solid lines show results from the present work on $NaFe_{0.935}Co_{0.045}As$. The red, blue, and black dashed regions show the range of 2Δ as determined from different ARPES and other experiments. In all cases, the resonance can be either below or above the 2Δ.

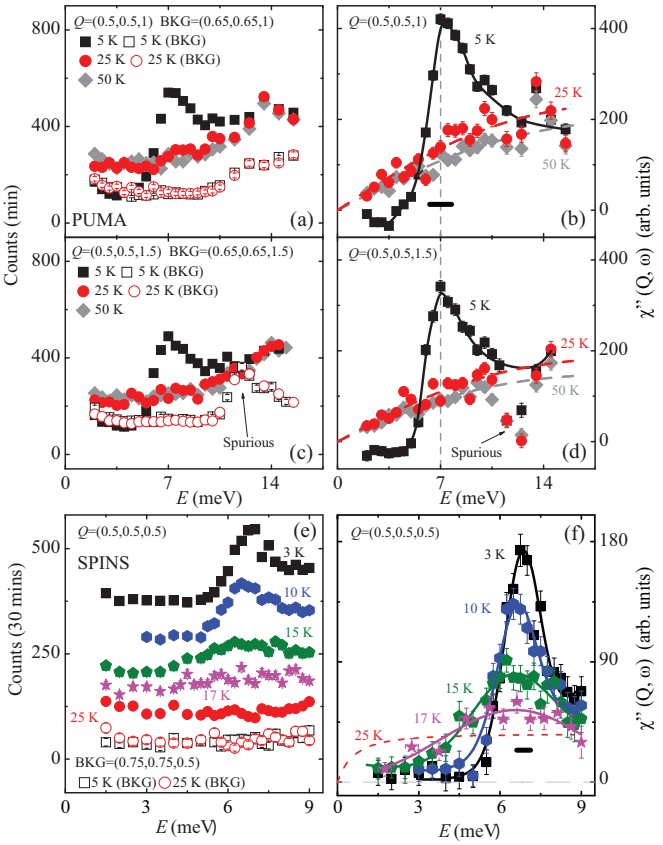

FIG. 2. (Color online) Energy scans at the AF wave vector. (a) and (c) Energy scans at $\mathbf{Q} = (0.5,0.5,1)$ and $\mathbf{Q} = (0.5,0.5,1.5)$, respectively, at 5, 25, and 50 K on PUMA. The background was taken at $\mathbf{Q} = (0.65,0.65,1)$ and $\mathbf{Q} = (0.65,0.65,1.5)$, respectively, at 5 and 25 K. (b) and (d) are the corresponding $\chi''(Q,E)$. (e) Energy scans at $\mathbf{Q} = (0.5,0.5,0.5)$ at 3, 10, 15, 17, and 25 K on SPINS. The background scans at $\mathbf{Q} = (0.75,0.75,0.5)$ between 5 and 25 K are also shown. For clarity, the energy scans at $\mathbf{Q} = (0.5,0.5,0.5)$ were shifted above background data by 30 at 25 K, 100 at 17 K, 150 at 15 K, 230 at 10 K, and 330 at 3 K. (f) is the corresponding $\chi''(Q,E)$. The solid and dashed lines are guides to the eyes. The horizontal bars indicate instrumental energy resolution.

in iron pnictides arises from orbital fluctuation mediated s^{++}-pairing superconductivity,[27,31–34] where one expects a broad spin excitation enhancement (neutron spin resonance) at an energy of $E \geqslant 2\Delta$ below T_c.[31–33] Given the current debates concerning the universality of the electron pairing symmetry in iron-based superconductors,[34–39] it is important to compare spin excitations in different classes of iron superconductors and determine if the resonance in these materials agrees with predictions of the $s^{\pm}$- and s^{++}-pairing symmetries.

In this paper, we present inelastic neutron-scattering results on single crystals of SC $NaFe_{0.935}Co_{0.045}As$ with $T_c = 18$ K [Figs. 1(a)–1(d)]. In the normal state, the imaginary part of the dynamic susceptibility, $\chi''(\mathbf{Q},E)$, at the AF wave vector increases linearly with increasing energy E. Upon entering into the low-temperature SC state, a spin gap opens below 5.5 meV and a sharp neutron spin resonance appears at $E = 7$ meV with an energy width of 1.5 ± 0.1 meV [Figs. 2(d) and 2(f)]. On warming to T_c, the resonance broadens in energy width but its central position does not follow the decreasing SC gap energy, different from the earlier work on electron-doped $BaFe_2As_2$.[15] By comparing the neutron-scattering results with a random-phase approximation (RPA) spin-susceptibility calculation within the s^{+-} and s^{++} pairings, we find that our data are

consistent with the s^{+-} symmetry in the low-temperature SC state and cannot be explained by the s^{++}-pairing symmetry.

II. RESULTS

We carried out inelastic neutron-scattering experiments on the thermal (PUMA) and cold (PANDA) triple-axis spectrometers at the FRM-II, TU Müchen, Germany,[14] and also on the SPINS cold triple-axis spectrometer at NIST Center for Neutron Research, Gaithersburg, Maryland.[11] For the experiments, we coaligned five pieces of self-flux grown $NaFe_{1-x}Co_xAs$ single crystals with a total mass of 5.5 g (mosaic about 3°) for PUMA and PANDA experiment. Samples were loaded in a closed cycle refrigerator with a low temperature capability of 2.5 K.

For SPINS measurements, we used ∼20 g of single crystals with mosaic less than 3°. The chemical compositions of the samples are determined as $Na_{1.06}Fe_{0.935}Co_{0.045}As$ by inductively coupled plasma atomic-emission spectroscopy, which has an accuracy of about 2%. Samples from different batches show almost identical chemical composition, which we denote as $NaFe_{0.935}Co_{0.045}As$. The wave vector $\mathbf{Q}$ at (q_x,q_y,q_z) in Å^{-1} is defined as $(H,K,L) = (q_xa/2\pi, q_ya/2\pi, q_zc/2\pi)$ reciprocal-lattice unit (r.l.u.) using the tetragonal unit cell (space group $P4/nmm$, $a = 3.921$ Å, $c = 6.911$ Å at 5 K). We used horizontal focusing pyrolytic graphite (PG) monochromator and analyzer with fixed final energies of $E_f = 14.7$ meV and $E_f = 5$ meV at PUMA and PANDA, respectively. For SPINS measurements, we used $E_f = 5$ meV with vertically focused monochromator and horizontally flat analyzer. Both the $[H,H,L]$ and $[H,K,0]$ scattering zones have been used in the experiments and the scan directions are marked in Fig. 1(b). To characterize the samples, we have carried out resistivity and dc magnetic susceptibility measurements using a commercial physical property measurement system and a superconducting quantum interference device (SQUID) magnetometer. Based on the early neutron-diffraction measurements,[40] AF Bragg peaks and low-energy spin excitations are expected to occur around the $(0.5,0.5,L)$ positions with $L = 0.5, 1.5, \ldots$ [Fig. 1(b)].

Figure 1(c) plots the in-plane resistivity ρ_{ab} measurement at zero field which gives $T_c = 18$ K. The inset shows the magnetic-field dependence of ρ_{ab} at 0 and 9 T, indicating a field-induced T_c suppression of ∼2 K. Figure 1(d) shows the magnetic susceptibility measurements on the sample again showing a $T_c = 18$ K. Given the known electronic phase diagrams of $NaFe_{1-x}Co_xAs$,[41–43] it is clear that our $NaFe_{0.935}Co_{0.045}As$ samples are in the slightly overdoped regime and do not have static AF order coexisting with superconductivity [Figs. 1(a)]. Our elastic neutron-diffraction scans through the AF Bragg peak positions are featureless and thus confirm this conclusion (see Fig. 7 in the Appendix for details). Figure 1(e) shows schematics of the resonance for optimally hole[11] and electron[13,15–17] doped iron pnictides, as well as iron chalcogenide Fe(Se,Te),[22–24] and the ranges of SC gaps for these materials as determined from ARPES and other techniques.[25–30,34] For comparison, we also show the SC gaps determined from ARPES for $NaFe_{0.95}Co_{0.05}As$.[45,46] As we can see, the ARPES measurements from two groups on $NaFe_{0.95}Co_{0.05}As$ have yielded SC gaps different by a factor of 2.

In previous neutron-scattering work on electron doped $BaFe_{2-x}Ni_xAs_2$ pnictide superconductors,[14,17] the neutron spin resonance was found to be dispersive, occurring at slightly different energies for different c-axis wave-vector transfers. To see if this is also the case for spin excitations in $NaFe_{0.935}Co_{0.045}As$, we carried out constant-$\mathbf{Q}$ scans at wave vectors $\mathbf{Q} = (0.5,0.5,1)$ and $(0.5,0.5,1.5)$ below and above T_c on PUMA. While the background scattering (BKG) taken at $\mathbf{Q} = (0.65,0.65,1)$ and $(0.65,0.65,1.5)$ showed no change below and above T_c [Figs. 2(a) and 2(c)], the scattering at the in-plane AF wave vector revealed dramatic changes across T_c. In the normal state ($T = 25$ K), the scattering above BKG is featureless and increases with increasing energy. Upon entering into the SC state ($T = 5$ K), a spin gap forms below ∼5.5 meV and a sharp resonance appears at $E = 7$ meV [Figs. 2(a) and 2(c)]. The corresponding $\chi''(Q,E)$, obtained by subtracting the BKG and correcting for the Bose population factors using $\chi''(Q,E) = [1 - \exp(-E/k_BT)]S(Q,E)$, are shown in Figs. 2(b) and 2(d). Inspection of Figs. 2(a)–2(d) reveals that the resonance exhibits no measurable c-axis dispersion and has a measured energy width of ∼3 meV full-width-at-half-maximum (FWHM). Figures 2(e) and 2(f) show similar scans on SPINS with better resolution, which reveal a 5-meV spin gap and a sharp resonance at $E = 6.8 \pm 0.1$ meV with an energy width of ∼1.5 meV in the SC state at 3 K. This is much narrower than the energy widths of the resonances in the hole and electron-doped $BaFe_2As_2$ [Fig. 1(e)].[10–19] On warming to 10, 15, and 17 K, the resonance energy widths become broader, but its peak position remains almost unchanged up to $T = 0.94T_c = 17$ K [Fig. 2(f)]. This is different from earlier work on the temperature dependence of the resonance energy in $BaFe_{1.85}Co_{0.15}As_2$ ($T_c = 25$ K),[15] but similar to the temperature dependence of the resonance in Fe(Se,Te) family of materials.[23,24]

To confirm the SC spin gap and determine the wave-vector dependence of the resonance, we carried out constant-energy scans at $E = 4,7$, and 15 meV below and above T_c. Figures 3(a)–3(c) and 3(d)–3(f) show $\chi''(Q,E)$ along the $[H,H,1]$ and $[H,H,1.5]$ directions, respectively. In the SC state at $T = 5$ K, $\chi''(Q,E)$ is featureless at $E = 4$ meV and thus confirms the presence of a spin gap. For other excitation energies, the scattering profiles can be fit by Gaussians on linear BKG. Taking the Fourier transforms of the fitted Gaussian peaks along the $[H,H,1]$ direction, we find that the in-plane spin-spin correlation lengths at the energy of the resonance are $\xi = 24 \pm 1$ Å at 25 K and $\xi = 30 \pm 1$ Å at 5 K. Along the $[H,H,1.5]$ direction, $\xi = 32 \pm 3$ Å is unchanged from 25 to 5 K. Increasing the excitation energy to $E = 15$ meV ($> 2\Delta$), there are no observable differences in scattering intensity and spin correlation lengths ($\xi = 20 \pm 1$ Å) below and above T_c.

Figure 4(a) shows the temperature dependence of the scattering at the AF wave vector $\mathbf{Q} = (0.5,0.5,1.5)$ for the resonance ($E = 7$ meV) and spin gap ($E = 4$ meV) energies. While the intensity increases dramatically below T_c at the resonance energy, it decreases at $E = 4$ meV signaling the opening of a SC spin gap. To test if spin excitations in $NaFe_{0.935}Co_{0.045}As$ are indeed two dimensional in reciprocal

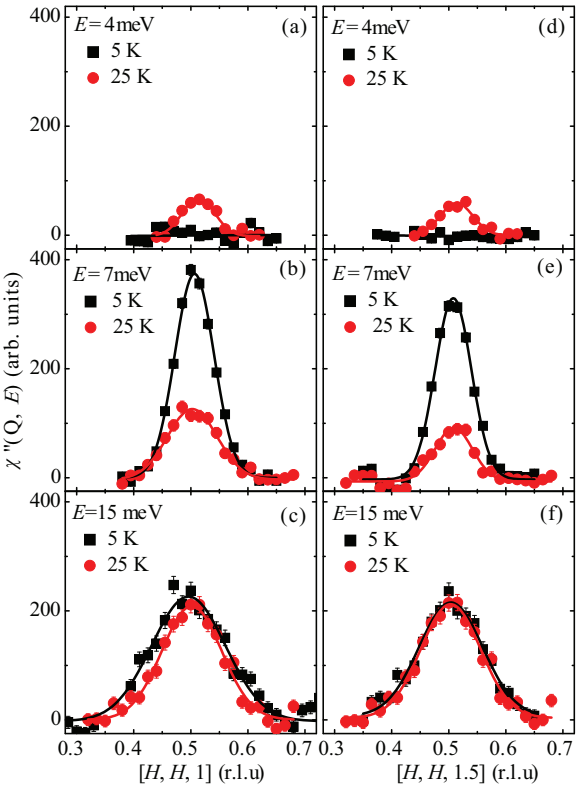

FIG. 3. (Color online) Constant-energy **Q** scans along the $[H,H,L = 1,1.5]$ directions below and above $T_c = 18$ K at different energies: (a),(d) in the gap (4 meV), (b),(e) at the resonance energy (7 meV), and (c),(f) well above 2Δ (15 meV). The solid lines are fits to Gaussians. Data are from PUMA.

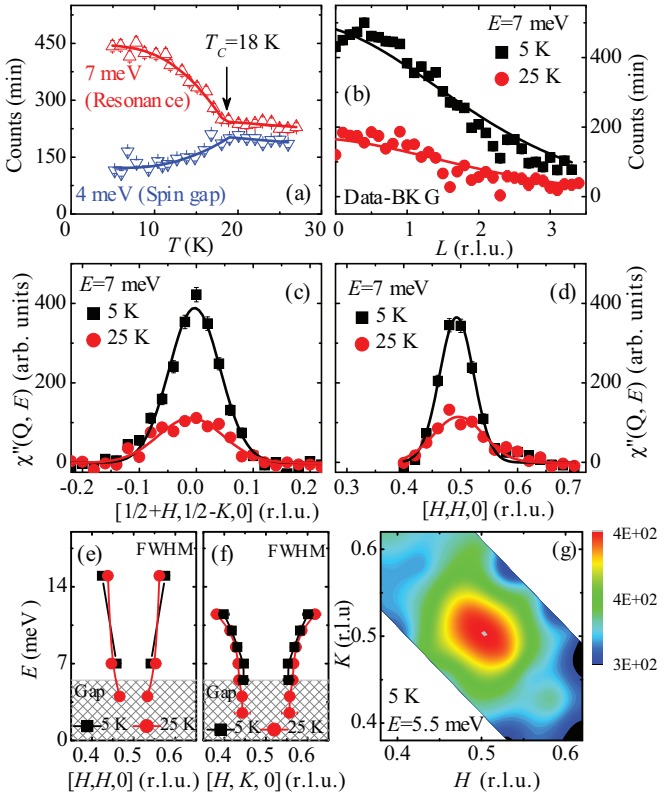

FIG. 4. (Color online) Temperature dependence of the resonance and spin gap. (a) Temperature dependence of the scattering at $\mathbf{Q} = (0.5,0.5,1.5)$ at $E = 4$, and 7 meV. The solid lines show the order-parameter fits by using $I = I_o + K[1 - (T/T_c)]^{\beta}$ yielding $T_c = 18.8$ K for both. (b) Background subtracted constant energy scans with $E = 7$ meV along the $[0.5,0.5,L]$ direction at 5 and 25 K. Background was taken at $\mathbf{Q} = (0.65,0.65,L)$. The solid lines are the square of the Fe^{2+} form factor. (c) and (d) **Q** scans below and above T_c along the $[1/2 + H,1/2 - H,0]$ and $(H,H,0)$ directions, respectively. (e) and (f) The dispersions of spin excitations below and above T_c along the $[H,H,0]$ and $[H - \delta,K + \delta,0]$ directions, respectively. The shaded area indicates the size of the spin gap in the SC state. (g) The in-plane wave vector profile of the $E = 5.5$-meV spin excitations in the SC state. Data are from PUMA.

space like in the case of Co-doped $BaFe_2As_2$,[13] we show in Fig. 4(b) BKG subtracted constant-energy scans along the $[0.5,0.5,L]$ direction at the resonance energy ($E = 7$ meV) below and above T_c. The monotonic decrease of the scattering with increasing L is consistent with the square of the Fe^{2+} magnetic form factor, thus confirming the two-dimensional and magnetic nature of the resonance.

In the optimally hole[11] and electron-doped $BaFe_2As_2$,[16,17,19] the resonances form longitudinally and transversely elongated ellipses, respectively. Since $NaFe_{0.935}Co_{0.045}As$ belongs to the electron-doped iron pnictide superconductor, we mapped out spin excitations in the $[H,K,0]$ scattering plane on PUMA. Figures 4(c) and 4(d) show constant-energy scans at $E = 7$ meV along the transverse $[1/2 + H,1/2 - H,0]$ and longitudinal $[H,H,0]$ directions [perpendicular and parallel to the in-plane AF ordering wave vector $\mathbf{Q} = (0.5,0.5,0)$], respectively, below and above T_c. Although there is no evidence for transverse incommensurate magnetic scattering as in the case of LiFeAs,[44] the spin resonance in $NaFe_{0.935}Co_{0.045}As$ is considerably broader along the transverse direction than that of the longitudinal direction. Figure 4(g) shows the two-dimensional image of the resonance in the SC state, further confirming the results of Figs. 4(c) and 4(d).

Figures 4(e) and 4(f) summarize FHWM of the low-energy spin excitations along the longitudinal and transverse directions below and above T_c, respectively. In the normal state, spin excitations in $NaFe_{0.935}Co_{0.045}As$ are gapless, comparing with the $\sim$10 meV anisotropy gap for spin waves of the undoped NaFeAs.[47] The data points are the FWHM of spin excitations along the two high-symmetry directions. On cooling to below T_c, the effect of superconductivity is to open a low-energy spin gap and concurrently form a neutron spin resonance. The dispersions of the spin excitations are essentially unaffected by superconductivity.

III. DISCUSSION AND CONCLUSIONS

To compare with the experiment, we have performed RPA spin-susceptibility calculations in the SC state, using the five-orbital tight-binding model taken from Ref. 48. The details of the calculations can be found in Ref. 49 and the Appendix. Results for the s^{+-}- and s^{++}-pairing symmetries are given in Figs. 5(a)–5(c). For $s^{\pm}$ pairing, a spin resonance appears due to the inelastic scattering of the Bogoliubov quasiparticles whose energy and wave vector can approximately be determined

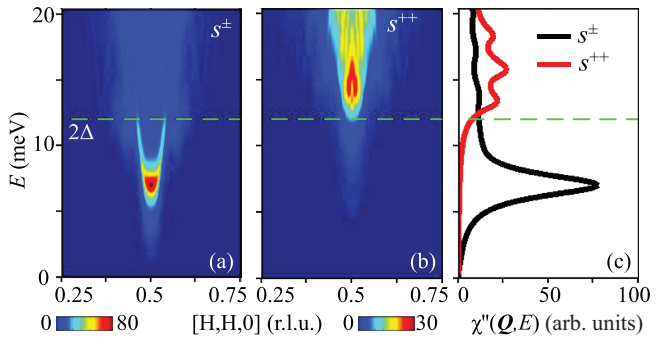

FIG. 5. (Color online) RPA calculated resonance for $s^{\pm}$- and s^{++}-pairing symmetries. (a) Computed spin-excitation spectrum for the $s^{\pm}$ pairing channel. (b) Same but for s^{++}-pairing symmetry. (c) $\chi''(\omega)$ at the AF wave vector $\mathbf{Q}$ for both these cases. The horizontal lines mark the $2\Delta_0$ line, below and above which the resonance occurs in the two cases, respectively. Both calculations are performed with fixed intrinsic broadening of 1 meV, SC gap of $\Delta_0 = 6$ meV, and Coulomb interaction $U = 1.6$ eV.

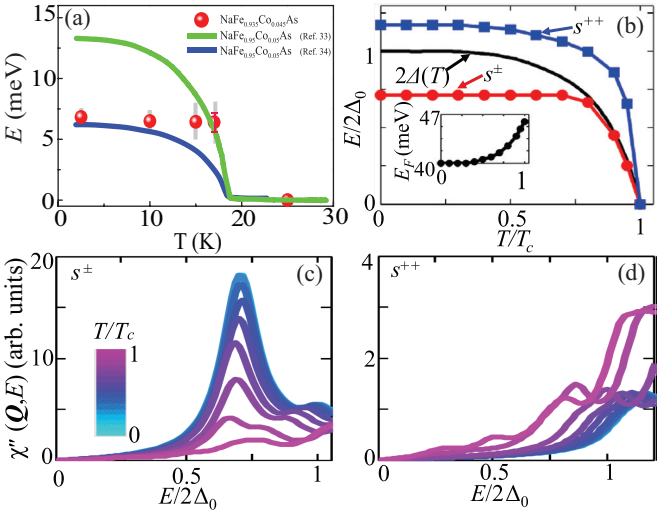

FIG. 6. (Color online) Temperature evolution of spin resonance for $s^{\pm}$- and s^{++}-pairing symmetries. (a) Temperature dependence of the peak position and energy width of the resonance, compared with temperature dependence of the SC gap energies as obtained from ARPES measurements [solid green (Ref. 45) and blue (Ref. 46) curves]. The vertical shaded bars are FWHM of the resonance. The error bars of the resonance peak energies are smaller than the symbol size for $T \leqslant 15$ K. (b) Self-consistent values of the spin-resonance energy E_{res} plotted as a function of temperature in the SC state for the two pairing symmetries under consideration, and compared with the SC gap amplitude. All energy scales are normalized by the SC gap value at $T = 0$, while the temperature is normalized by T_c for presentation. The spin resonance for $s^{\pm}$ pairing remains very much temperature independent except near T_c due to self-consistently evaluated change in the Fermi level (shown in the inset) at each temperature, while that for the s^{++} pairing follows the gap function at each temperature. (c) Spin-resonance peak position and intensity as a function of energy at the commensurate wave vector at different temperatures (see the color scale) for $s^{\pm}$ pairing symmetry. (d) Same as (c) but for the s^{++}-pairing symmetry. Contrasting evolution of the resonance energy and intensity can be marked between $s^{\pm}$ and s^{++} pairing, and our experimental data are consistent with the former pairing symmetry results.

from $E = |\Delta^{\nu}_{\mathbf{k}_F}| + |\Delta^{\nu'}_{\mathbf{k}_F+\mathbf{Q}}|$ given that $\mathrm{sgn}[\Delta^{\nu}_{\mathbf{k}}] \neq \mathrm{sgn}[\Delta^{\nu'}_{\mathbf{k}+\mathbf{Q}}]$ between band indices ν and ν', where $\Delta^{\nu}_{\mathbf{k}} = \Delta^{\nu}_0 g(\mathbf{k})$ with $g(\mathbf{k}) = (\cos k_x + \cos k_y)$. There are two reasons for the resonance shift to $E < 2\Delta_0$: (1) Due to the large area of the electron pocket in these systems,[45] the effective gap value of the Fermi momenta is reduced, i.e., $|g(\mathbf{k}_F)| < 1$. (2) The resonance energy shifts further to lower energy within RPA.[49] We take $\Delta_0 \approx 6$ meV (Ref. 45) to obtain a resonance at 7 meV, in accord with the experimental value. For the s^{++} pairing, due to the lack of sign reversal, the spin excitations inside the SC gap are completely eliminated. However, at $E > 2\Delta_0$, a humplike feature in intensity appears. The many-body RPA correction shifts the hump to a higher energy [for the same value of $U = 1.6$ meV, we obtain a weak feature around $E = 1.3(2\Delta)$], as shown in Figs. 5(b) and 5(c). With varying U as well as the intrinsic broadening, we find that the result is robust and the $s^{\pm}$ resonance peak is ubiquitously sharper than that for the s^{++} case. Therefore, our low-temperature neutron-scattering results in Fig. 2 are only consistent with $s^{\pm}$-pairing symmetry regardless of the actual values of the SC gaps.[45,46]

On the other hand, assuming that temperature dependence of the SC gaps in $NaFe_{0.935}Co_{0.045}As$ follows the BCS form, as demonstrated in many pnictide superconductors,[34,35] we observe that the resonance energy remains very much temperature independent; see Fig. 6(a). To explain this behavior, we calculate the temperature evolution of the spin susceptibility and the results are shown in Figs. 6(b)–6(d). For each temperature, we evaluate the Fermi energy (E_F) constrained by the fixed number of electrons. As shown in the inset to Fig. 6(b), E_F increases as the gap decreases with temperature. The corresponding change in the Fermi surface topology yields a change in the effective gap value for $s^{\pm}$ pairing due to the anisotropic gap structure factor $g(\mathbf{k})$ defined before. Additionally, this leads to a reduction in χ' in the $s^{\pm}$-pairing state, and for the temperature-independent interaction U, the resonance condition shifts to a higher energy, as illustrated in the Appendix. Due to the interplay between these two changes as a function of temperature, the resonance energy shifts to higher energy compared to its corresponding $2\Delta(T)$ value, but remains very much temperature independent with respect to its $2\Delta(0)$ energy [Fig. 6(a)]. This analysis does not apply to the s^{++}-pairing symmetry since it is insensitive to the change in the underlying Fermi surface. Therefore, the resonance energy in this pairing symmetry, which lies above $2\Delta(T)$, very much follows the gap function.

The corresponding line shape of the resonance is shown in Figs. 6(c) and 6(d) for $s^{\pm}$ and s^{++}, respectively. The contrasting temperature evolution of χ'' at the commensurate wave vector can be marked between the two pairing symmetries. For $s^{\pm}$ pairing, the resonance intensity decreases according to the BCS prediction, but its position does not shift in energy until the temperature reaches the vicinity of T_c, where the resonance shifts to lower energy below its corresponding $2\Delta(T)$. On the contrary, for s^{++} pairing the resonance intensity increases and gradually shifts to lower energy. This contrasting behavior can be understood from the physics of the resonance described in the Appendix. As shown

there, the weak intensity hump above the 2Δ for s^{++} arises from the discontinuous jump in the particle-hole channel in the SC region. As the gap decreases, the energy scale of the jump also decreases, and thus the resonance energy follows the gap evolution, and remains almost insensitive to the modification in the underlying electronic structure.

In summary, we have discovered a sharp resonance in electron-overdoped $NaFe_{0.935}Co_{0.045}As$ in the low-temperature SC state. Our experimental data are only consistent with the $s^{\pm}$-pairing state both in terms of intensity and energy scales, and thus provide unambiguous evidence for the presence of $s^{\pm}$-pairing symmetry in pnictide superconductors.

ACKNOWLEDGMENTS

The single-crystal growth efforts and neutron-scattering work at UT/Rice were supported by the US DOE, BES, through Contract No. DE-FG02-05ER46202. Work at IOP was supported by MOST (973 Project No. 2012CB82400). The work at JCNS and RWTH Aachen University was partially funded by the BMBF under Contract No. 05K10PA3. Work at LANL was supported by the NNSA of the US DOE under Contract No. DE-AC52-06NA25396. Work at SYSU was supported by NSFC-11074310, RFDPHE-20110171110026, NCET-11-0547.

APPENDIX

In this Appendix, we first present elastic neutron-diffraction data on the sample and then give the details of our calculations presented in the main text. The elastic neutron-scattering scans across the AF Bragg peak positions are featureless and thus confirm this conclusion that the material does not have static AF order (see Fig. 7).

We evaluate the spin-resonance susceptibility in the superconducting (SC) state within the BCS-RPA formalism[49,50] which is given by

$$\chi^{rstu}_{BCS}(\mathbf{q},\omega) = \frac{1}{N}\sum_{\boldsymbol{k}} M^{\nu,\nu'}_{rstu}(\boldsymbol{k},\boldsymbol{q}) \left\{ \frac{1}{2}\left[1 + \frac{\xi^{\nu}_{\boldsymbol{k}}\xi^{\nu'}_{\boldsymbol{k}+\boldsymbol{q}} + \Delta^{\nu}_{\boldsymbol{k}}\Delta^{\nu'}_{\boldsymbol{k}+\boldsymbol{q}}}{S^{\nu}_{\boldsymbol{k}}S^{\nu'}_{\boldsymbol{k}+\boldsymbol{q}}}\right]\frac{f(S^{\nu}_{\boldsymbol{k}}) - f(S^{\nu'}_{\boldsymbol{k}+\boldsymbol{q}})}{\omega - S^{\nu}_{\boldsymbol{k}} + S^{\nu'}_{\boldsymbol{k}+\boldsymbol{q}} + i\delta} \right.$$
$$+ \frac{1}{4}\left[1 + \frac{\xi^{\nu}_{\boldsymbol{k}}}{S^{\nu}_{\boldsymbol{k}}} - \frac{\xi^{\nu'}_{\boldsymbol{k}+\boldsymbol{q}}}{S^{\nu'}_{\boldsymbol{k}+\boldsymbol{q}}} - \frac{\xi^{\nu}_{\boldsymbol{k}}\xi^{\nu'}_{\boldsymbol{k}+\boldsymbol{q}} + \Delta^{\nu}_{\boldsymbol{k}}\Delta^{\nu'}_{\boldsymbol{k}+\boldsymbol{q}}}{S^{\nu}_{\boldsymbol{k}}S^{\nu'}_{\boldsymbol{k}+\boldsymbol{q}}}\right]\frac{1 - f(S^{\nu}_{\boldsymbol{k}}) - f(S^{\nu'}_{\boldsymbol{k}+\boldsymbol{q}})}{E + S^{\nu}_{\boldsymbol{k}} + S^{\nu'}_{\boldsymbol{k}+\boldsymbol{q}} + i\delta}$$
$$\left. + \frac{1}{4}\left[1 - \frac{\xi^{\nu}_{\boldsymbol{k}}}{S^{\nu}_{\boldsymbol{k}}} + \frac{\xi^{\nu'}_{\boldsymbol{k}+\boldsymbol{q}}}{S^{\nu'}_{\boldsymbol{k}+\boldsymbol{q}}} - \frac{\xi^{\nu}_{\boldsymbol{k}}\xi^{\nu'}_{\boldsymbol{k}+\boldsymbol{q}} + \Delta^{\nu}_{\boldsymbol{k}}\Delta^{\nu'}_{\boldsymbol{k}+\boldsymbol{q}}}{S^{\nu}_{\boldsymbol{k}}S^{\nu'}_{\boldsymbol{k}+\boldsymbol{q}}}\right]\frac{f(S^{\nu}_{\boldsymbol{k}}) + f(S^{\nu'}_{\boldsymbol{k}+\boldsymbol{q}}) - 1}{E - S^{\nu}_{\boldsymbol{k}} - S^{\nu'}_{\boldsymbol{k}+\boldsymbol{q}} + i\delta}\right\}. \quad \text{(A1)}$$

Here $S^{\nu}_{\boldsymbol{k}} = [(\xi^{\nu}_{\boldsymbol{k}})^2 + (\Delta^{\nu}_{\boldsymbol{k}})^2]^{1/2}$ is the SC quasiparticle state for the eigenstate $\xi^{\nu}_{\boldsymbol{k}}$ (ν is the band index) and the SC gap $\Delta^{\nu}_{\boldsymbol{k}}$. For $s^{\pm}$-pairing symmetry we have $\Delta^{\nu}_{\boldsymbol{k}} = \Delta^{\nu}_0(\cos k_x + \cos k_y)$ and for s^{++} wave pairing symmetry we take $\Delta^{\nu}_{\boldsymbol{k}} = \Delta^{\nu}_0$ to be the same for all bands. M is the matrix element consisting of the eigenstates of the initial and final scattered quasiparticle state as given by $M^{\nu,\nu'}_{rstu}(\boldsymbol{k},\boldsymbol{q}) = \phi^{\nu'\dagger}_r(\boldsymbol{k}+\boldsymbol{q})\phi^{\nu}_s(\boldsymbol{k})\phi^{\nu\dagger}_t(\boldsymbol{k})\phi^{\nu'}_u(\boldsymbol{k}+\boldsymbol{q})$, where $\phi^{\nu}_r(\boldsymbol{k})$ is the eigenfunction of the νth band derived from the rth orbital.

In Eq. (A1), the first term is called the particle-hole scattering term which vanishes in the SC state due to particle-hole symmetry regardless of any pairing symmetry. The second and third terms are called particle-particle and hole-hole scatterings, respectively, which become active in the SC state. Focusing on the third term (the same analysis applies to the second term), we find that this term contributes a nonzero value only when $\mathrm{sgn}[\Delta^{\nu}_{\boldsymbol{k}}] \neq \mathrm{sgn}[\Delta^{\nu'}_{\boldsymbol{k}+\boldsymbol{q}}]$ (since $\xi^{\nu}_{\boldsymbol{k}} = 0$ on the Fermi

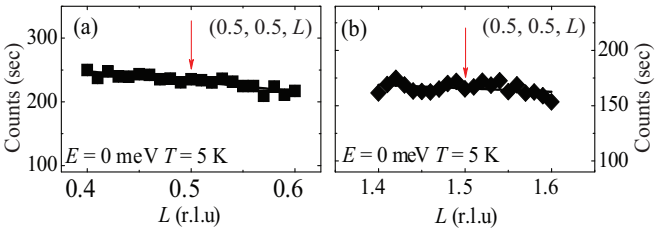

FIG. 7. (Color online) Elastic neutron scattering through the AF Bragg positions. (a),(b) Elastic neutron scattering from PUMA along the [0.5,0.5,L] directions at 5 K. The solid lines are guides to the eye and the arrows indicate the positions of AF static ordering.

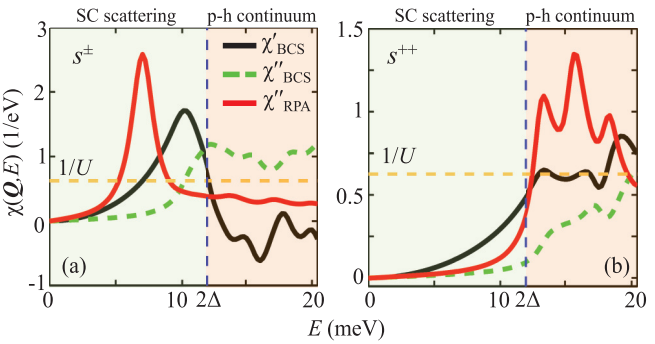

FIG. 8. (Color online) (a) Various components of the spin susceptibility are plotted together for $s^{\pm}$ pairing. The RPA value of the susceptibility (red line) is very sharp (of the order of 100 eV^{-1}), and thus we divide it by 30 to fit it into the same figure or visualization. For the same reason, the real part of the bare susceptibility χ'_{BCS} is subtracted from its zero energy value and multiplied by 4.9 and the imaginary part of the BCS susceptibility is multiplied by 2. (b) Same as (a) but for s^{++} pairing. Here χ''_{RPA} is divided by 20 and χ''_{BCS} is multiplied by 2. The horizontal dashed line gives $1/U$, which illustrated the occurrence of the resonance mode when it cuts through χ'_{BCS}. Finally, the vertical dashed line marks the 2Δ line which separates the SC scattering region to the p-h continuum.

surface). A pole is thus obtained in the imaginary part of χ_{BCS} at

$$E = \left|\Delta_{\boldsymbol{k}}^{\nu}\right| + \left|\Delta_{\boldsymbol{k}+\boldsymbol{q}}^{\nu'}\right|. \tag{A2}$$

(Of course, many-body effects and matrix-element effects can shift the energy scale as discussed below.) For s^{++} pairing, the lack of sign reversal prevents any resonance to occur inside the gap. Here, for $E > 2\Delta$ Eq. (A1) transforms into the particle-hole (p-h) channel governed by the free-fermion Lindhard function as

$$\chi_0^{rstu}(\boldsymbol{q},E) = \frac{1}{N}\sum_{\boldsymbol{k}} M_{rstu}^{\nu,\nu'}(\boldsymbol{k},\boldsymbol{q})\frac{f\left(\xi_{\boldsymbol{k}}^{\nu}\right) - f\left(\xi_{\boldsymbol{k}+\boldsymbol{q}}^{\nu'}\right)}{E - \xi_{\boldsymbol{k}}^{\nu} + \xi_{\boldsymbol{k}+\boldsymbol{q}}^{\nu'} + i\delta}. \tag{A3}$$

Unlike the BCS susceptibility, the p-h continuum is considerably broader and is obtained from the dynamical nesting between different bands as $E_q = \xi_{\boldsymbol{k}}^{\nu} - \xi_{\boldsymbol{k}+\boldsymbol{q}}^{\nu'}$. For $s^{\pm}$ pairing, χ_{BCS} gives a very sharp resonance feature inside the SC region, which virtually washes out the information of the p-h continuum above this energy scale. On the other hand, for s^{++} pairing, $\chi_{BCS} = 0$ and the sharp crossover to χ_0 at $E = 2\Delta$ acts as an abrupt change in the real part of χ_0. In both cases, the Fermi-surface nesting between electron pockets sitting at the M point and the hole pockets at the Γ point is most dominant, giving features at the commensurate wave vector $\boldsymbol{Q} = (0.5,0.5)$. The characteristic differences in the bare susceptibilities for the two pairing channels are given in Fig. 8.

We include the many-body correction to the spin-excitation spectrum via standard RPA formalism as $\tilde{\chi}_{RPA} = \tilde{\chi}_{BCS}/(\tilde{1} - \tilde{U}\tilde{\chi}_{BCS})$, where the tilde symbol over a quantity represents that it is a matrix in the orbital basis (see Fig. 8). The interaction vertex consists of intraorbital Coulomb interaction U and interorbital term $V = 2U' - J$, where $U' = U - 5/4J$ and $J = U/8$ is the Hund's coupling and $J' = J/2$ is the pair hopping term. For a single band system, a spin resonance occurs when the denominator of the RPA susceptibility vanishes at $\chi'_{BCS} = 1/U$, and the peak is broadened by χ''_{BCS}. The situation is equivalent, yet complicated in the multiorbital case. We obtain a sharp resonance peak for the $s^{\pm}$-pairing case below 2Δ where the broadening associated with χ''_{BCS} is much reduced, as shown in Fig. 8(a). On the other hand, for s^{++} the resonance in the p-h continuum is broadened by a large value of χ''_0 [see the green dashed line in Fig. 8(b)].

*pdai@rice.edu

[1] C. C. Tsuei and J. R. Kirtley, Rev. Mod. Phys. **72**, 969 (2000).

[2] Y. Kamihara, T. Watanabe, M. Hirano, and H. Hosono, J. Am. Chem. Soc. **130**, 3296 (2008).

[3] M. Rotter, M. Tegel, and D. Johrendt, Phys. Rev. Lett. **101**, 107006 (2008).

[4] C. W. Chu, F. Chen, M. Gooch, A. M. Guloy, B. Lorenz, B. Lv, K. Sasmal, Z. J. Tang, J. H. Tapp, and Y. Y. Xue, Physica C **469**, 326 (2009).

[5] I. I. Mazin, D. J. Singh, M. D. Johannes, and M. H. Du, Phys. Rev. Lett. **101**, 057003 (2008).

[6] K. Kuroki, S. Onari, R. Arita, H. Usui, Y. Tanaka, H. Kontani, and H. Aoki, Phys. Rev. Lett. **101**, 087004 (2008).

[7] K. Seo, B. A. Bernevig, and J. P. Hu, Phys. Rev. Lett. **101**, 206404 (2008).

[8] M. M. Korshunov and I. Eremin, Phys. Rev. B **78**, 140509(R) (2008).

[9] T. A. Maier and D. J. Scalapino, Phys. Rev. B **78**, 020514(R) (2008).

[10] A. D. Christianson, E. A. Goremychkin, R. Osborn, S. Rosenkranz, M. D. Lumsden, C. D. Malliakas, I. S. Todorov, H. Claus, D. Y. Chung, M. G. Kanatzidis, R. I. Bewley, and T. Guidi, Nature (London) **456**, 930 (2008).

[11] C. Zhang, M. Wang, H. Luo, M. Wang, M. Liu, J. Zhao, D. L. Abernathy, T. A. Maier, K. Marty, M. D. Lumsden, S. Chi, S. Chang, J. A. Rodriguez-Rivera, J. W. Lynn, T. Xiang, J. Hu, and P. Dai, Sci. Rep. **1**, 115 (2011).

[12] J.-P. Castellan, S. Rosenkranz, E. A. Goremychkin, D. Y. Chung, I. S. Todorov, M. G. Kanatzidis, I. Eremin, J. Knolle, A. V. Chubukov, S. Maiti, M. R. Norman, F. Weber, H. Claus, T. Guidi, R. I. Bewley, and R. Osborn, Phys. Rev. Lett. **107**, 177003 (2011).

[13] M. D. Lumsden, A. D. Christianson, D. Parshall, M. B. Stone, S. E. Nagler, G. J. MacDougall, H. A. Mook, K. Lokshin, T. Egami, D. L. Abernathy, E. A. Goremychkin, R. Osborn, M. A. McGuire, A. S. Sefat, R. Jin, B. C. Sales, and D. Mandrus, Phys. Rev. Lett. **102**, 107005 (2009).

[14] S. Chi, A. Schneidewind, J. Zhao, L. W. Harriger, L. Li, Y. Luo, G. Cao, Z. Xu, M. Loewenhaupt, J. Hu, and P. Dai, Phys. Rev. Lett. **102**, 107006 (2009).

[15] D. S. Inosov, J. T. Park, P. Bourges, D. L. Sun, Y. Sidis, A. Schneidewind, K. Hradil, D. Haug, C. T. Lin, B. Keimer, and V. Hinkov, Nat. Phys. **6**, 178 (2010).

[16] C. Lester, J.-H. Chu, J. G. Analytis, T. G. Perring, I. R. Fisher, and S. M. Hayden, Phys. Rev. B **81**, 064505 (2010).

[17] J. T. Park, D. S. Inosov, A. Yaresko, S. Graser, D. L. Sun, Ph. Bourges, Y. Sidis, Y. Li, J.-H. Kim, D. Haug, A. Ivanov, K. Hradil, A. Schneidewind, P. Link, E. Faulhaber, I. Glavatskyy, C. T. Lin, B. Keimer, and V. Hinkov, Phys. Rev. B **82**, 134503 (2010).

[18] J. Zhao, L.-P. Regnault, C. Zhang, M. Wang, Z. Li, F. Zhou, Z. Zhao, C. Fang, J. Hu, and P. Dai, Phys. Rev. B **81**, 180505(R) (2010).

[19] M. Liu, L. W. Harriger, H. Luo, M. Wang, R. A. Ewings, T. Guidi, H. Park, K. Haule, G. Kotliar, S. M. Hayden, and P. Dai, Nat. Phys. **8**, 376 (2012).

[20] D. S. Inosov, J. T. Park, A. Charnukha, Y. Li, A. V. Boris, B. Keimer, and V. Hinkov, Phys. Rev. B **83**, 214520 (2011).

[21] P. Dai, J. Hu, and E. Dagotto, Nat. Phys. **8**, 709 (2012).

[22] H. A. Mook, M. D. Lumsden, A. D. Christianson, S. E. Nagler, B. C. Sales, R. Jin, M. A. McGuire, A. S. Sefat, D. Mandrus, T. Egami, and C. de la Cruz, Phys. Rev. Lett. **104**, 187002 (2010).

[23] Y. Qiu, W. Bao, Y. Zhao, C. Broholm, V. Stanev, Z. Tesanovic, Y. C. Gasparovic, S. Chang, J. Hu, B. Qian, M. Fang, and Z. Mao, Phys. Rev. Lett. **103**, 067008 (2009).

[24] L. W. Harriger, O. J. Lipscombe, C. Zhang, H. Luo, M. Wang, K. Marty, M. D. Lumsden, and P. Dai, Phys. Rev. B **85**, 054511 (2012).

[25] P. Richard, T. Sato, K. Nakayama, T. Takahashi, and H. Ding, Rep. Prog. Phys. **74**, 124512 (2011).

[26]K. Terashima, Y. Sekiba, J. H. Bowen, K. Nakayama, T. Kawahara, T. Sato, P. Richard, Y.-M. Xu, L. J. Li, G. H. Cao, Z.-A. Xu, H. Ding, and T. Takahashi, Proc. Natl. Acad. Sci. USA **106**, 7330 (2009).

[27]D. V. Evtushinsky, D. S. Inosov, V. B. Zabolotnyy, A. Koitzsch, M. Knupfer, B. Buchner, M. S. Viazovska, G. L. Sun, V. Hinkov, A. V. Boris, C. T. Lin, B. Keimer, A. Varykhalov, A. A. Kordyuk, and S. V. Borisenko, Phys. Rev. B **79**, 054517 (2009).

[28]W. Malaeb, T. Shimojima, Y. Ishida, K. Okazaki, Y. Ota, K. Ohgushi, K. Kihou, T. Saito, C. H. Lee, S. Ishida, M. Nakajima, S. Uchida, H. Fukazawa, Y. Kohori, A. Iyo, H. Eisaki, C.-T. Chen, S. Watanabe, H. Ikeda, and S. Shin, Phys. Rev. B **86**, 165117 (2012).

[29]F. Hardy, P. Burger, T. Wolf, R. A. Fisher, P. Schweiss, P. Adelmann, R. Heid, R. Fromknecht, R. Eder, D. Ernst, H. v. Löhensey, and C. Meingast, Europhys. Lett. **91**, 47008 (2010).

[30]L. Luan, T. M. Lippman, C. W. Hicks, J. A. Bert, O. M. Auslaender, J.-H. Chu, J. G. Analytis, I. R. Fisher, and K. A. Moler, Phys. Rev. Lett. **106**, 067001 (2011).

[31]S. Onari, H. Kontani, and M. Sato, Phys. Rev. B **81**, 060504(R) (2010).

[32]S. Onari and H. Kontani, Phys. Rev. B **84**, 144518 (2011).

[33]Y. Nagai and K. Kuroki, Phys. Rev. B **83**, 220516(R) (2011).

[34]S. V. Borisenko, V. B. Zabolotnyy, A. A. Kordyuk, D. V. Evtushinsky, T. K. Kim, I. V. Morozov, R. Follath, and B. Büchner, Symmetry **4**, 251 (2012).

[35]P. J. Hirschfeld, M. M. Korshunov, and I. I. Mazin, Rep. Prog. Phys. **74**, 124508 (2011).

[36]A. Chubukov, Annu. Rev. Condens. Matter Phys. **3**, 57 (2012).

[37]J. P. Hu, Phys. Rev. X **3**, 031004 (2013).

[38]R. M. Fernandes and A. J. Millis, Phys. Rev. Lett. **110**, 117004 (2013).

[39]E. Dagotto, Rev. Mod. Phys. **85**, 849 (2013).

[40]S. Li, C. de la Cruz, Q. Huang, G. F. Chen, T.-L. Xia, J. L. Luo, N. L. Wang, and P. Dai, Phys. Rev. B **80**, 020504(R) (2009).

[41]D. R. Parker, M. J. P. Smith, T. Lancaster, A. J. Steele, I. Franke, P. J. Baker, F. L. Pratt, M. J. Pitcher, S. J. Blundell, and S. J. Clarke, Phys. Rev. Lett. **104**, 057007 (2010).

[42]A. F. Wang, X. G. Luo, Y. J. Yan, J. J. Ying, Z. J. Xiang, G. J. Ye, P. Cheng, Z. Y. Li, W. J. Hu, and X. H. Chen, Phys. Rev. B **85**, 224521 (2012).

[43]G. Tan, P. Zheng, X. Wang, Y. Chen, X. Zhang, J. Luo, T. Netherton, Y. Song, P. Dai, C. Zhang, and S. Li, Phys. Rev. B **87**, 144512 (2013).

[44]N. Qureshi, P. Steffens, Y. Drees, A. C. Komarek, D. Lamago, Y. Sidis, L. Harnagea, H.-J. Grafe, S. Wurmehl, B. Büchner, and M. Braden, Phys. Rev. Lett. **108**, 117001 (2012).

[45]Z.-H. Liu, P. Richard, K. Nakayama, G.-F. Chen, S. Dong, J.-B. He, D.-M. Wang, T.-L. Xia, K. Umezawa, T. Kawahara, S. Souma, T. Sato, T. Takahashi, T. Qian, Y. Huang, N. Xu, Y. Shi, H. Ding, and S.-C. Wang, Phys. Rev. B **84**, 064519 (2011).

[46]S. Thirupathaiah, D. V. Evtushinsky, J. Maletz, V. B. Zabolotnyy, A. A. Kordyuk, T. K. Kim, S. Wurmehl, M. Roslova, I. Morozov, B. Büchner, and S. V. Borisenko, Phys. Rev. B **86**, 214508 (2012).

[47]J. T. Park, G. Friemel, T. Loew, V. Hinkov, Yuan Li, B. H. Min, D. L. Sun, A. Ivanov, A. Piovano, C. T. Lin, B. Keimer, Y. S. Kwon, and D. S. Inosov, Phys. Rev. B **86**, 024437 (2012).

[48]S. Graser, T. A. Maier, P. J. Hirschfeld, and D. J. Scalapino, New J. Phys. **11**, 025016 (2009).

[49]T. Das and A. V. Balatsky, Phys. Rev. Lett. **106**, 157004 (2011).

[50]T. A. Maier, S. Graser, D. J. Scalapino, and P. Hirschfeld, Phys. Rev. B **79**, 134520 (2009).